Optimization of the processing parameters for the preparation of dip-coated CuO photocathodes and modification with Au nanoparticles for water-splitting

Nteseng D. M. Mosalakgotla[1], Pannan I. Kyesmen[1] and Mmantsae Diale[1]

[1]*Department of Physics, University of Pretoria, Private Bag X20, Hatfield 0028, South Africa*

Corresponding author e-mail addresses: pannan.kyesmen@up.ac.za: mmantsae.diale@up.ac.za

Abstract

Here, the processing parameters for preparing dip-coated CuO photocathodes such as withdrawal velocity, film thickness, and calcination temperature were optimized for photoelectrochemical (PEC) applications. CuO films were prepared at varying withdrawal rates between 50-200 mm/min, made to consist of 239.7-693.6 ± 40 nm film thicknesses, and annealed at 400-650°C for 1 hr. Furthermore, Au nanoparticles (Au NPs) were deposited on the CuO films that were prepared at 150 mm/min withdrawal velocity, 432.8 ± 27 nm thick, and treated at 600°C to protect the films against photo-corrosion during PEC reactions. The prepared films were confirmed to be of high purity via Raman spectroscopy and X-ray diffraction (XRD) studies. The maximum photocurrent density of 2.9 mA/cm^2 at 0.35 V vs RHE was obtained for the CuO photocathodes prepared at 150 mm/min withdrawal velocity, with the thickness of 432.8 nm, and treated at 600°C. The high photocurrent density has been linked to the combine effect of the optimization of film thickness, optical absorbance, crystallization, and the low resistance to charge transfer at the photocathode/electrolyte junction exhibited by the films. The deposition of Au NPs on the pristine CuO photocathodes resulted in a 62 % drop in their photocurrent density due to the inhibition of high photo-corrosion occurring on the film's surface. A potential-time scan at 0.6 V vs RHE for 500 s yielded a 3-fold improvement in the photo-stability of the Au coated films in electrolyte over the pristine CuO photocathodes. This study emphasized the role of optimizing multiple processing parameters in the fabrication of CuO photocathodes before the deposition of protective layers for water splitting applications.

Keywords: Dip-coated CuO photocathodes, film processing parameters, Au nanoparticles, PEC water-splitting.

1. Introduction.

Over the years, the increasing concentration of greenhouse gases, mainly CO_2 has been linked to the growing global population and the consumption of non-renewable energy sources [1]. This has prompted investigations in sustainable renewable energy sources aimed at using them to substitute the utilization of conventional fossil fuels. The production of liquid fuels such as hydrogen, methanol, methane, etc., via renewable means, has attracted great research interest in recent years. Hydrogen fuel has emerged as one of the most versatile, efficient, environmentally friendly, inexpensive, and the best transportation fuel due to its high power density and the by-product of water and oxygen after combustion [2]. Due to these realities, there is a great demand for clean hydrogen-generating technologies. Dincer *et. al, 2015* investigated the electrical, thermal, biochemical, and photonic-based hydrogen-generating sources, where the photonic hydrogen-generating sources which include the PEC techniques, were found to be the most eco-friendly [3].

PEC water splitting is a technique that has attracted global research interest in recent years because of its application in harvesting solar energy for the production of hydrogen fuel [4]. Materials with a small bandgap for sufficient light-harvesting, suitable band positions for H_2 and O_2 evolution, high diffusion length, and efficient charge separation are desired for effective PEC water splitting [5-7]. Semiconductors such as copper oxide (CuO), cuprous oxide (Cu_2O), delafossite ($CuFeO_2$), calcium iron oxide ($CaFe_2O_4$), and kusachiite ($CuBi_2O_4$) photocathodes [4, 8] have been engaged in a PEC cell to split water into its constituent elements. CuO photocathodes have the advantage of affordability [9], small bandgap (1.2 – 1.51 eV) [10], abundance [4, 11], and suitable band position for H_2 evolution reactions during PEC water splitting [12]. The preparation techniques of CuO photocathodes can have a significant influence on their properties such as photon absorption, crystallization, and surface chemical reactions, thus influencing the efficiency of the overall PEC process [5, 13]. Techniques such as hydrothermal [5], electrodeposition [14], chemical vapour deposition [15], spray pyrolysis [16], and sol-gel dip-coating [9] have been used for preparing CuO nanostructures for photocatalytic applications. Among these methods, the sol-gel dip-coating is captivating due to its low processing cost, ease of processing, composition control, as well as its ability to form uniform films on substrates with large surface areas [9, 17].

The processing parameters of preparing nanostructured CuO films using the sol-gel dip-coating method such as withdrawal rate, film thickness, and annealing temperature can influence the optical, structural, and photocatalytic properties of the films [16, 18, 19]. Withdrawal velocity

has been found to influence the grain size [20] and thickness [18] of the films. An increasing film thickness may improve crystallinity [16], which limits the probability of electron-hole recombination, promoting efficient charge separation and migration [21, 22]. Increasing annealing temperature has also been reported to enhance the crystallinity of the films [23], limit grain boundaries and improve their photo-absorption, which is essential for an efficient water-splitting process [22]. The influence of withdrawal rates on the PEC properties of photoelectrodes such as CuO has been carried out [24]. However, a study on the influence of withdrawal velocity on the PEC response of CuO photocathodes is yet to be reported. Also, separate investigations have been conducted on the effects of film thickness [25] and calcination temperature [26] on the structural, photo-absorption, and electrical properties of dip-coated CuO films for various applications. However, based on known literature, a single study where withdrawal rates, calcination temperature, and the film's thickness were optimized for dip-coated CuO photocathodes for photocatalytic water splitting have not been reported.

In this research, the processing parameters of preparing nanostructured CuO films which include the withdrawal velocity, calcination temperature, and film thickness, were investigated for the advancement of PEC H_2 generation reaction. The CuO photocathodes were fabricated on FTO substrates at 50-200 mm/min withdrawal rates, with 239.7–693.6 ± 40 nm thicknesses, and annealed at temperatures between 400-650°C for 1 hr. In addition, Au NPs were deposited on the pristine CuO films that were 432.8 ± 27 nm thick to serve as protective layers against photo-corrosion during PEC reactions. The highest photocurrent density of 2.9 mA/cm^2 at 0.35 V vs RHE was obtained for the CuO photocathodes prepared at 150 mm/min withdrawal velocity, with the thickness of 432.8 ± 27 nm, and treated at 600°C. The coating of Au NPs on the pristine CuO photocathodes yielded a 3-fold improvement in their photo-stability in electrolyte after a potential-time scan at 0.6V vs RHE for 500 s. This study underscores the role of optimizing multiple processing parameters in the fabrication of CuO photocathodes prior the deposition of protective layers for photocatalytic applications.

2. Experimental

2.1. CuO thin films preparation

The copper acetate-based precursor solution used for the CuO film deposition on FTO substrates was made following a method described in our previous work [27]. The FTO

substrates were cleaned via sonication in deionized (DI) water, detergent, methanol, and isopropanol for 15 min each, and dried with nitrogen (N_2) gas. CuO samples were fabricated on the cleaned FTO substrates using sol-gel dip-coating and a three-step heat treatment approach while varying withdrawal velocity, film thickness and calcination temperature. To optimize the withdrawal rate, the substrates were dipped into the precursor solution for 1 min and withdrawn at different velocities of 50, 100, 150, and 200 mm/min, respectively. The deposited films were then dried for 12 min at 120°C and for an additional 5 min at 300°C. This process was repeated for four more times to obtain 5 layers of the films prepared at the different withdrawal rates earlier mentioned. The films were all annealed for 1 hr at 600°C for further crystallization. To optimize the film thickness, more CuO samples were fabricated at 150 mm/min withdrawal rate to consist of 7 and 10 layers. The films were also prepared under the same drying and annealing conditions as the ones prepared at different withdrawal rates. Lastly, more CuO films were also prepared at the withdrawal velocity of 150mm/min, made to consist of 7 film layers, and subjected to the same drying and heat treatment conditions as previous samples except that they were calcined at 400°C, 500°C, and 650°C to study the influence of sintering temperature on the photocatalytic response of the films. An illustration of the experimental procedure for the CuO films preparation is given in Fig. 1.

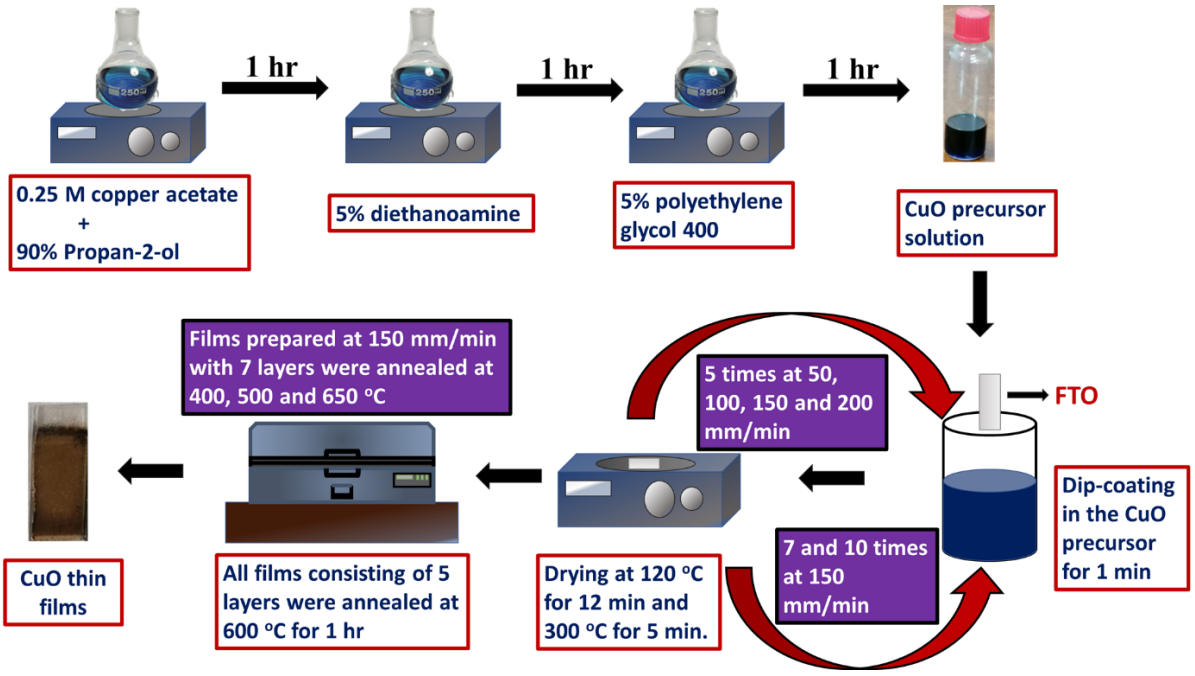

Fig. 1. Schematic diagram illustrating the procedure for the preparation of CuO films.

2.2. CuO/Au films preparation

CuO films prepared at withdrawal speed of 150 mm/min, consisting of 7 layers and annealed at 600°C were further modified with Au NPs using a simple solution-based drop casting technique. The precursor solution used for the Au NPs deposition was prepared by adding 40 mM $NaBH_4$ into a stirring solution containing 1mM of Chloroauric acid ($HAuCl_4$) and 1 mM of $Na_3C_6H_50_7$ in DI water. This resulted in the mixture immediately turning into a light shade of pink colour. After 20 minutes of heating while stirring at 100°C, the solution turned to a ruby-red colour, indicating the formation of Au NPs. The ruby-red solution was heated for an additional 10 mins at the same temperature to obtain a solution of Au NPs. Furthermore, 150 µL of the prepared Au NPs solution was added dropwise onto the pristine CuO films via the drop casting technique. The films were then allowed to dry on a hot plate at 100°C for 15 min to obtain 1 layer of Au NPs on CuO films. The drop casting procedure was repeated twice to obtain 3 layers of deposited Au nanoparticles on the pristine CuO films and labelled as CuO/Au.

2.3. Characterization.

The structural properties of the prepared CuO and CuO/Au photocathodes were examined using XRD measurements with a D2 PHASER-e diffractometer which uses Cu-Kα radiation at the wavelength of 0.15418 nm. The Raman spectra of the films were analysed using WiTec alpha 300 RAS+ Confocal Raman equipment with a 532 nm laser at 5 mW. The Field Emission Scanning Electron Microscopy (FE-SEM) was used to study the surface morphology and cross-section of the prepared films using the Zeiss Ultrafast 540 instrument. An energy dispersive X-ray spectroscopy (EDS) system which was attached to the Zeiss Crossbeam 540 instrument was used to analyse the elemental composition of the thin films. The Agilent Cary 60 UV-Vis spectrometer was used employed to investigate the optical behaviour of the films.

2.4. PEC measurements

The PEC responses of the prepared CuO and CuO/Au photocathodes were examined using a PEC cell consisting of three electrodes and a VersaSTAT 3F potentiostat. The PEC cell used to perform the PEC measurements consist of a transparent window made of fused silica (amorphous SiO_2) for transmission of simulated sunlight radiation [28]. 1M NaOH (pH = 13.6)

bubbled with N_2 gas for 30 mins was used as the electrolyte for the electrochemical measurements. The CuO photocathodes served as the working electrodes while Ag/AgCl in 3M KCl and 2 × 2 cm platinum mesh were used as the reference and counter electrodes respectively. The photocurrent responses of the films were obtained using linear scan voltammetry (LSV) measurements which were performed on the CuO working electrodes at 0.04 V/s scan rate, in both dark and light settings. The Newport *Oriel LCS* −100 TM solar simulator was used as the illumination source and calibrated using a Newport 91150V standard cell to 1 sun. The surface area of the working electrodes exposed to the simulated solar illumination was $0.49cm^2$. Electrochemical impedance spectroscopy (EIS) analysis was performed to investigate the charge transfer kinetics processes occurring at the surface of the photocathodes. These were carried out under dark conditions at -0.5 V vs. Ag/AgCl, at an excitation amplitude of 10 mV, and a frequency range of 10 000 – 0.1 Hz. ZView software was used to perform an equivalent circuit fitting of the EIS data that were obtained for the photocathodes. Chronoamperometry measurements were also performed in both dark and light settings to investigate the photostability of CuO photocathodes at -0.4 V vs Ag/AgCl for a period of 400 s. All potentials measured vs Ag/AgCl standard were transformed to the RHE reference using the Nernst relation in equation 1:

$$\Phi_{RHE} = \Phi Ag/AgCl + (0.059 \times pH) + \Phi^{o}Ag/AgCl \text{ vs SHE} \quad (1)$$

where Φ_{RHE} represents the potential in RHE scale, $\Phi Ag/AgCl$ stand for the potential vs the Ag/AgCl reference electrode, and $\Phi^{o}Ag/AgCl$ vs SHE stands for the reference electrode potential represented against the standard hydrogen potential (SHE) which has a value of 0.198 V at 25 ℃ [28, 29].

3. Results and discussion

3.1. Structural properties

Structural information of the CuO and CuO/Au photocathodes were extracted from the XRD studies done between 2 theta values of 20-80° and the results are given in Fig. 2 (a), (b), and (c) for samples prepared at different withdrawal rates, with varying thicknesses and sintered at various temperatures respectively. Diffraction peaks were seen on the XRD patterns at $(\bar{1}11)$ and (111) planes which confirmed the monoclinic crystal structure of the CuO with lattice parameters a = 4.64 Å, b = 3.4 Å, c = 5.09 Å, β = 99.5° according to JCPDS file number 05–

0661 [16, 29]. Less intense XRD peaks were also seen at (020) and ($\bar{1}$13) corresponding to those of CuO films. No obvious peak shifts were observed and new peaks for Cu or Cu_2O were also not seen in the XRD pattern, which confirmed the good purity of the CuO films prepared. The intensity of the diffraction peaks increases with increasing withdrawal velocity as seen in Fig 2(a). This was due to the increase in the thickness of the films with increasing withdrawal velocity [30]. Films with different number of deposited layers also exhibited an increase in their XRD peak intensities as a result of increasing film thickness [31]. Films consisting of seven layers which were annealed at different temperatures also show enhancement in their XRD peak intensities due to increasing sintering temperature. This is attributed to the improvement in the crystallinity of the thin films with increasing annealing temperature [16, 23]. The XRD pattern of the CuO/Au films also revealed diffraction peaks at ($\bar{1}$11) and (111) planes for the monoclinic crystal structure of CuO films (Fig. 2(d)). In addition, the diffraction peaks attributed to Au at (111), (200), (220), and (311) planes emerged for the samples, confirming the face-centered cubic structure of Au, with a lattice constant a = 4.077 Å, according to the JCPDS no. 01-071-3755 [69, 70].

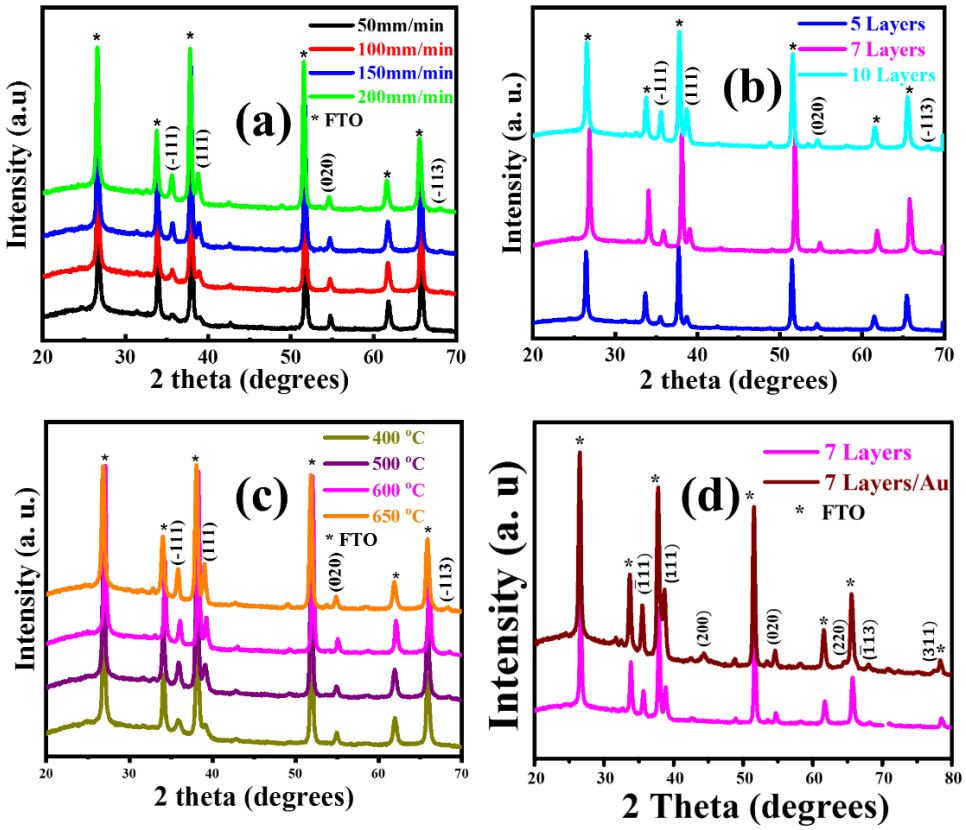

Fig. 2. XRD pattern of CuO samples **(a)** withdrawn from the precursor at different velocities, **(b)** consisting of varying number of film layers, and **(c)** annealed at various temperatures: **(d)** compares the XRD pattern of the pristine CuO and CuO/Au films.

The XRD peaks at ($\bar{1}11$) were used to estimate the full width at half maximum (FWHM) and crystal size (D) values of the prepared CuO and CuO/Au samples. This was done to investigate the impact of withdrawal velocity, calcination temperature, and film thickness on the crystallization of the films. The Debye-Scherrer relation in Eq. (2) was employed to calculate the estimated crystal size values for the CuO samples [29].

$$D = \frac{k\lambda}{B\cos\theta} \tag{2}$$

where k has a constant value of 0.9, λ = 0.15418 nm for the Cu-Kα X-ray source, β is the estimated FWHM value and θ represent the Bragg angle [32].

The FWHM and crystal size values of the CuO films prepared at different withdrawal rates, consisting of samples with varying number of film layers, and annealed at various temperatures are given in Table 1. For films prepared using different withdrawal velocities, the films which were withdrawn at 150 mm/min and 50 mm/min were observed to have the highest and least crystal sizes of 19.4 and 8.5 nm respectively. An increasing crystal size value for the thin films is an indication of improved crystallization. For the optimization of film thickness, the withdrawal velocity of 150 mm/min was used to prepare the CuO films consisting of various number of film layers because of the high crystallinity observed for the films. This was due to the crucial role that high film crystallization has on PEC water-splitting as it promotes efficient charge migration and separation [33]. There was no significant change in the crystal sizes of the films consisting of different layers since they were all annealed at the same temperature of 600°C. Similarly, the deposition of a thin layer of Au NPs on the pristine CuO films had no significant influence on their crystal sizes. Lastly, the films sintered at 650°C had the highest crystallite size of 21.01 nm. This may be due to the increase in thermal energy by the particles with increasing annealing temperature which promotes migration of atoms during crystal formation, leading to larger crystallites [23]. Thin films with good crystallinity are desired for PEC applications because of their role in promoting charge mobility during photocatalytic reactions [34].

Table 1. XRD analysis showing the FWHM and crystal sizes of CuO and CuO/Au thin films prepared using different processing parameters.

Processing parameters	**Sample**	**2 theta (degrees)**	**FWHM**	**Crystal size (nm)**
Withdrawal velocity	**50 mm/min**	35.66	0.89	8.50
	100 mm/min	35.62	0.63	12.01
	150 mm/min	35.68	0.39	19.40
	200 mm/min	35.80	0.41	18.45
Film thickness	**5 Layers**	35.68	0.39	19.04
	7 Layers	36.08	0.38	19.89
	10 Layers	35.76	0.37	20.44
	7 Layers/Au	35.50	0.37	20.46
Annealing temperature	**400°C**	35.89	0.76	9.96
	500°C	35.93	0.49	15.43
	600°C	36.08	0.38	19.89
	650°C	35.84	0.36	21.01

The Raman spectra for the CuO and CuO/Au samples were obtained to study the phonon vibrational modes of the films in order to extract more structural information from the films. The spectra are shown in Fig. 3 (a), (b) and (c) for samples prepared at different withdrawal rates, consisting of varying film layers and annealed at various temperatures respectively. The Raman spectra disclosed the 1Ag vibrational phonon modes at 302 cm^{-1}, and the 2Bg ones at 250 and 638 cm^{-1} respectively, which are all associated with CuO. The modes for Cu, Cu_2O, or other oxides of Cu were not present in the spectra, further affirming the good quality of the prepared CuO samples. Raman peak intensities of the CuO samples increases with increment in the withdrawal velocity from 50 – 150 mm/min due to increasing film's crystallization. The film withdrawn at 200 mm/min did not show much change in its Raman intensity compared to those prepared at 150 mm/min because there was no significant difference in their crystallinity (Table 1). The Raman peaks of CuO films consisting of 5-10 layers did not show any significant difference in their intensities. This was because the films had similar crystallinity as observed in their XRD analysis (Table 1). Fig. 3(c) reveals a more broadened Raman peaks for films

prepared at low annealing temperatures caused by the quantum confinement effect of the CuO nanoparticles [35]. The Raman spectra of the CuO/Au films revealed the $1A_g$ and $2B_g$ phonon modes for CuO. In addition, peaks at 773, 1124, 1185, 1364, 1507 and 1546 cm^{-1} belonging to the phonon modes of AuNPs were also observed, further confirming the presence of Au on the pristine CuO films.

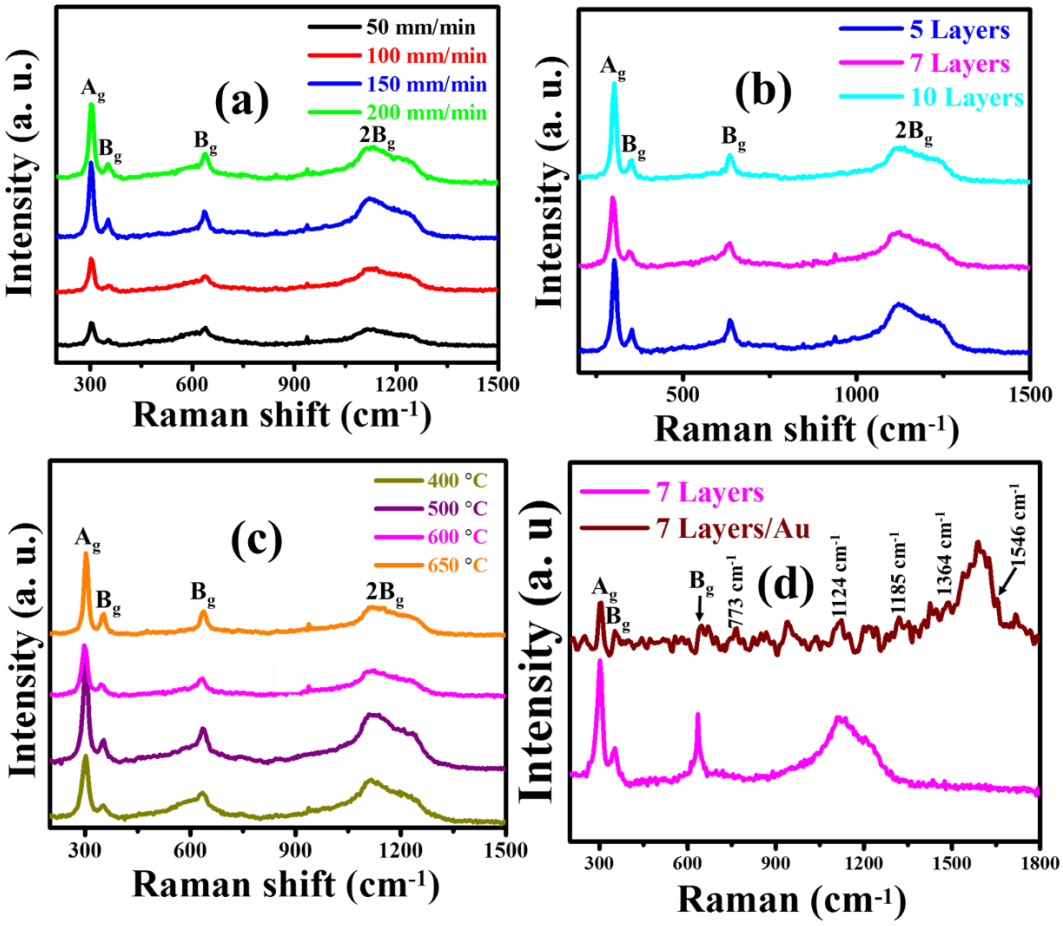

Fig. 3. Raman spectra of CuO photocathodes **(a)** withdrawn from the precursor at different velocities, **(b)** consisting of different number of film layers, and **(c)** annealed at different temperatures: (d) compares the Raman spectra of the pristine CuO and CuO/Au films.

3.2. Surface morphology and film thickness

The prepared CuO films were characterized using FE-SEM to understand the impact of various sample processing parameters on their surface morphology. The morphology of the CuO thin films prepared at different withdrawal rates, with varying thicknesses, and sintered at various

temperatures all revealed spherical nanoparticles which are homogeneously distributed throughout the substrates. Fig. 4 (a)-(d) presents the surface morphology of CuO films prepared at 50-200 mm/min withdrawal velocities respectively**.** The average grain sizes for the thin films withdrawn at 50, 100, 150, and 200 mm/min velocities were estimated as 19.60, 20.49, 25.13, and 25.82 nm with the standard deviation (SD) of 6.76, 10.16, 9.52, and 8.89 nm respectively. A slight increase in the porosity of films prepared at withdrawal velocities of 150 and 200 mm/min was observed. According to Brinker *et. al.*, 1991, an increase in the withdrawal speed results in an enhancement of the film's thickness, and thicker films take time to dry, leading to the stiffening of the films, consequently increasing porosity [30].

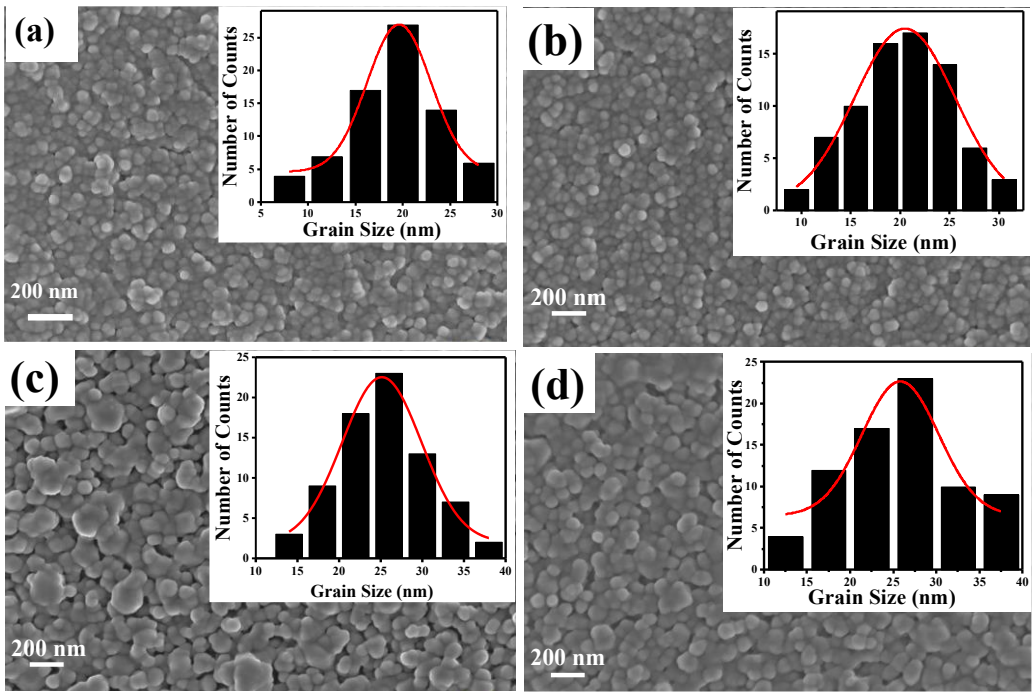

Fig. 4. FE-SEM micrographs of CuO thin films prepared at withdrawal velocities of **(a)** 50 mm/min **(b)** 100 mm/min **(c)** 150 mm/min **(d)** 200 mm/min: the corresponding histograms of the particle size distribution of the films are presented in their insets, respectively.

The surface morphology of CuO films with varying number of film layers are presented in Fig. S1 of the supplementary document for samples consisting of 5, 7, and 10 layers, prepared at 150 mm/min respectively. The surface of the films tends to be more porous with increasing number of film layers. There is no observed difference in the grain sizes of the films. The estimated mean values for the grain sizes of the CuO samples which were deposited with 5, 7, and 10 layers were estimated as 25.13, 26.37, and 24.92 nm with SD values of 9.52, 9.19, and

3.03 nm, respectively. The surface morphology of the CuO/Au films is shown in Fig. S1(d) of the supplementary document and revealed spherical CuO nanoparticles which have been largely covered with densely packed Au NPs. The grain sizes of CuO/Au films could not be evaluated due to the high agglomeration of the Au NPs on CuO films. The Au NPs deposited on the CuO films annealed at 600°C will serve as a protective layer for the films against photo-corrosion during PEC reactions.

The surface morphologies of the CuO samples calcined at various temperatures are also given in Fig. S2 of the supplementary information for the samples treated between 400-650°C. The grain sizes approximated for the films increased with increasing calcination temperature. The surface of the films sintered at 650°C looked more compact, smooth, and extremely agglomerated as compared to the ones treated at 400, 500, and 600°C. Furthermore, the nanoparticles seem to have coalesced into larger nanostructures which may be due to the large amount of tension over the surface of the films caused by the high annealing temperature [36]. The grain sizes approximated for the films treated at 400, 500, and 600°C was estimated as 12.85, 19.92, and 26.37 nm with the SD values of 3.85, 5.67, and 9.91 nm, respectively. The mean value for the grain sizes of the thin films treated at 650°C could not be estimated due to the extreme agglomeration and grain boundaries that are not well defined for the films.

The FE-SEM cross-sectional images of CuO thin samples made of 5 film layers and prepared at 50, 100, 150, and 200 mm/min withdrawal rates were obtained to estimate their thicknesses and are presented in Fig 5 (a), (b), (c) and (d) respectively. The average thicknesses of the films were estimated using ImageJ software to be 239.7 ± 23, 277.3 ± 32, 317.4 ± 40, and 355.2 ± 22 nm for samples prepared at 50, 100, 150, and 200 mm/min withdrawal velocities respectively. The thickness of the films increases with increasing withdrawal rates. This was as a result of the dragging caused by the viscous precursor solution on the moving substrate at higher withdrawal velocities during the dip-coating process [37]. The enhancement of thickness with increasing withdrawal rates also corresponds with the improvement in crystal sizes observed in the XRD analysis of the films (Table 1). This is similar to other observations in literature where increasing film thickness resulted in the enhancement of crystal size [38, 39].

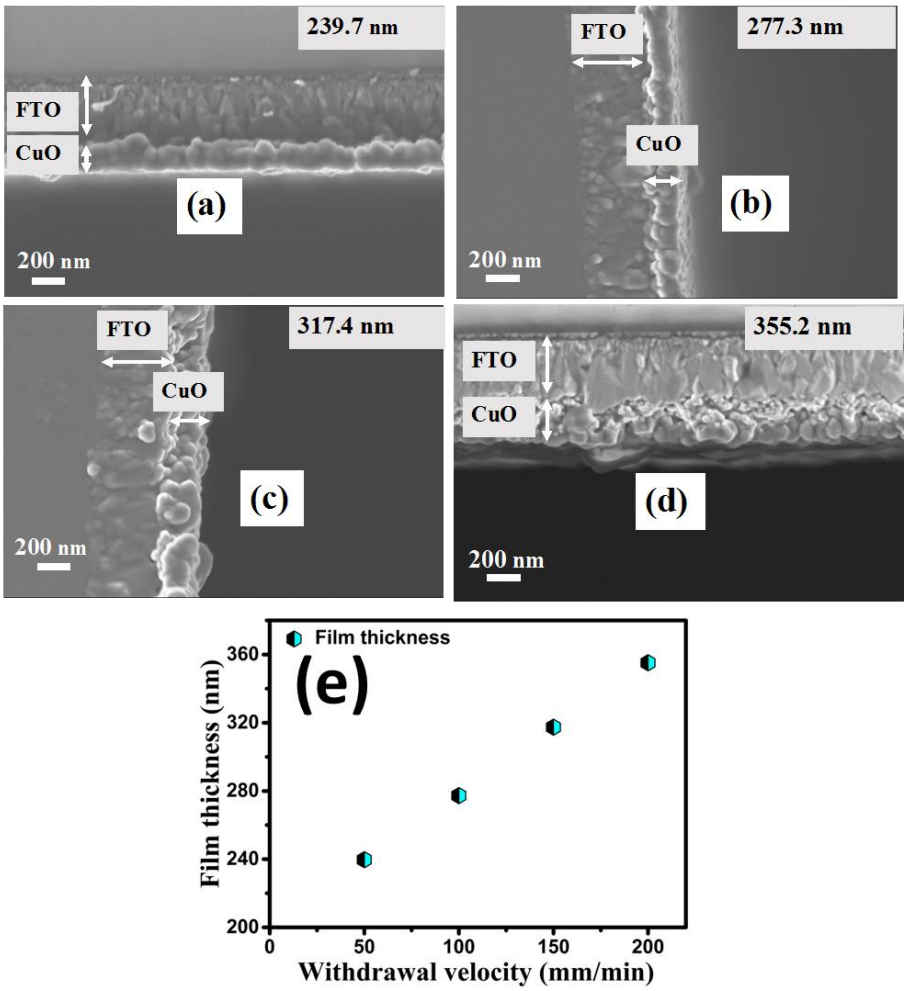

Fig. 5. FE-SEM cross-sectional images of CuO thin films prepared using withdrawal velocities of **(a)** 50 mm/min, **(b)** 100 mm/min, **(c)** 150 mm/min, and **(d)**200 mm/min.

The thickness of the films increases with the withdrawal rate as shown in Fig 5 (e) against intuitive thinking. This behaviour is supported by the theoretical considerations for the film thickness, d, of dip-coated films given by the Landau-Levich relation presented in eq. (3):

$$d = c \times \frac{(\eta U)^{2/3}}{\gamma^{1/6}(\rho g)^{1/2}} \qquad (3)$$

where c is a constant for Newtonian liquid which is equivalent to 0.944, η denotes the viscosity of the liquid, U represents the withdrawal velocity, γ is the surface tension of the liquid against air, ρ stand for the density of the liquid density and g is the acceleration due to gravity. This theory concludes that the d increases for the films with withdrawal velocity because of the radical function in U. In this theory, some features of the sol-gel film formation such as gelation

and the evaporation of the precursor were neglected; however, it gives a reasonable idea of the main parameters that covers the process of film formation [40, 41].

The FE-SEM cross-sectional images of the CuO samples prepared at 150 mm/min withdrawal velocity, consisting of 5, 7, and 10 layers are given in Fig. S3 of the supplementary document. The thickness of the CuO films was estimated to be 317.4 ± 40, 432.8 ± 27, and 693.6 ± 35 nm for films that had 5, 7, and 10 layers respectively. As anticipated, the approximated film thickness of the samples became larger with the addition of film layers. The cross-sectional view of the CuO/Au films given in Fig. S3(d) of the supplementary document disclosed an average film thickness of 55.84 ± 12 nm for the Au nanoparticles. The film thickness of the CuO samples that had 7 layers and annealed at 400, 500, and 650°C were not estimated since the annealing temperature was not expected to have a meaningful effect on the thickness of the films. This was because each layer of the films was treated at 120 and 300°C prior to annealing. In addition, Akgul *et. al, 2014* previously reported uniform thicknesses for CuO films which were sintered at various temperatures [23].

3.3. Elemental composition

The elemental compositions of the films were confirmed using EDS to check if impurities are present in the films. Fig. 6 (a), (b), (c), and (d) shows the results of the EDS analysis done on CuO samples prepared at withdrawal velocities of 50, 100, 150, and 200 mm/min, respectively. The analysis confirms the presence of oxygen (O) and copper (Cu) as expected since they were the constituent elements of CuO. Also, tin (Sn) and a little quantity of silicon (Si) were seen in the EDS analysis of all the films. The Sn observed in the films resulted from the SnO_2 content of the FTO substrates used for the film's deposition, while the Si detected was because of the quarts content of glass in the glass/FTO substrates [29]. The EDS analysis done on CuO films prepared at 150 mm/min which had different film layers and those of films annealed at various temperatures are given in Fig. S4 and S5 of the supplementary document respectively. As expected, the results all confirmed the same elemental composition as observed for CuO films prepared at different withdrawal velocities. The EDS analysis of CuO/Au shown in Fig. S4 (d) of the supplementary data also verifies the presence of Au for the films, aside from the O, Cu, Sn and Si elements observed, which have been associated to the deposited CuO films on glass/FTO substrates.

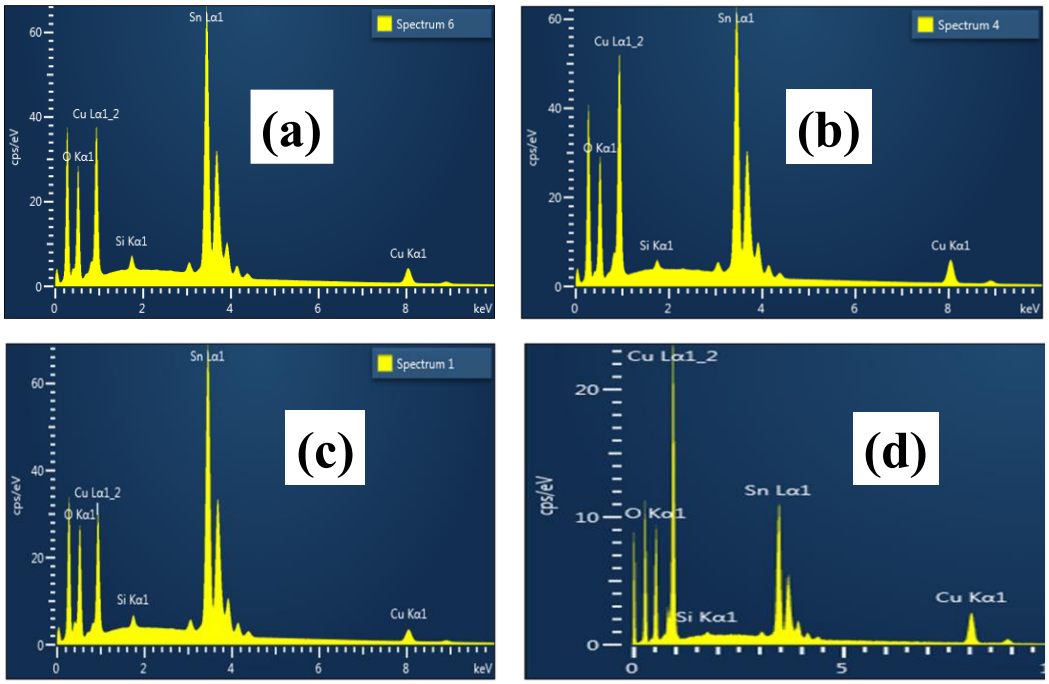

Fig. 6. EDS analysis of CuO thin films withdrawn from the precursor at **(a)** 50 mm/min, **(b)** 100 mm/min, **(c)** 150 mm/min, and **(d)** 200 mm/min velocities.

3.4. Optical properties

UV-Vis spectroscopy studies were done to investigate the optical absorption, transmittance, and indirect bandgap of the CuO thin films. Fig. 7 (a), (b), and (c) presents the optical absorption of the CuO samples prepared at several withdrawal rates, consisting of different number of film layers and sintered at various temperatures, respectively. The CuO thin films largely absorb in the visible spectrum, with a slight absorption in the near-infrared portion. The absorption of the CuO films increases with increasing withdrawal velocity (Fig. 7 (a)) and the number of film layers (Fig. 7 (b)) which are both related to the enhancement of the film's thickness [18]. Also, improved absorption was noticed for the CuO films with increasing calcination temperature (Fig. 7 (c)). Enhanced photo-absorbance in the visible region will lead to the increased production of electron-hole pairs, which can help in promoting PEC reactions [9]. The photo-absorbance of the CuO/Au films given in Fig. 7(d) improved when compared to that of the pristine CuO films. This was similar with other photo-absorption results that have been reported for the films in literature [69]. This may be attributed to the increased scattering of photons caused by the presence of the Au NPs on the CuO films surface. The transmittance

behaviours of the pristine CuO and CuO/Au films presented in the insets of Fig. 7 (a)-(d) are all in good agreement with their absorption patterns as expected.

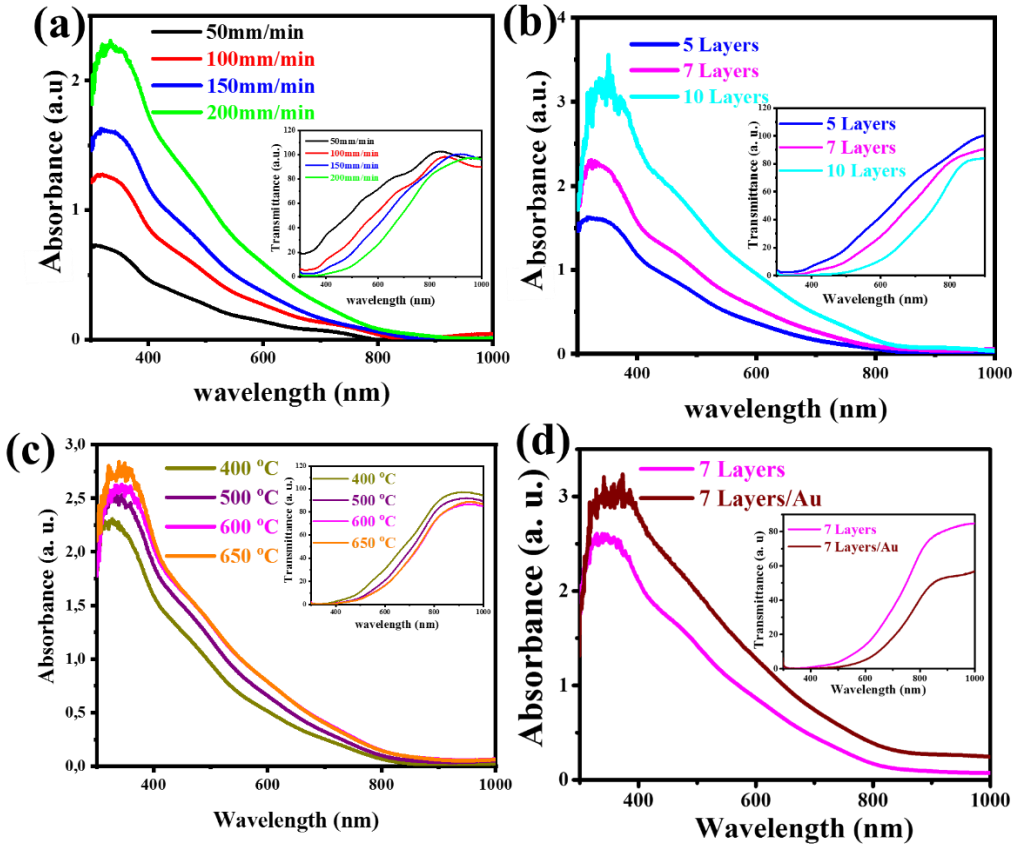

Fig. 7. UV-Vis absorption spectra of CuO thin films **(a)** withdrawn from the precursor at different velocities, **(b)** made consist of various number of film layers, and **(c)** annealed at several temperatures: (d) compares the photo-absorption of the pristine CuO and CuO/Au films. The inset of the figures shows the transmittance measurements of the films respectively.

The Tauc plots for the indirect transitions of the CuO photocathodes prepared at several withdrawal velocities, deposited to contain different number of film layers, and annealed at various temperatures are represented in Fig. 8 (a), (b), and (c) respectively. The plots were derived from the absorption spectra of the films and were used to approximate the values of their optical bandgaps (Eg) using the Tauc relation given in eq. (4) [42]:

$$^{\alpha}h\upsilon = A(h\upsilon - E_g)^n \qquad (4)$$

where α denote the absorption coefficient, *hv* represents the photon energy, A is a characteristic parameter that is independent of photon energy, Eg stands for the optical bandgap, and $n = \frac{1}{2}$

for direct transition and = 2 for indirect transition [18, 23]. The indirect bandgaps for the films were estimated to be 1.34 ± 0.04 eV for all the pristine CuO films. The indirect bandgaps estimated for the films are low when compared to the values reported for the films in some literatures [16, 31]. The bandgap of the CuO films further reduced to an estimated value of 1.20 ± 0.03 eV after modification with Au NPs (Fig. 8(d)). Low bandgaps are associated with the wide range of photo-absorbance in the visible region which can positively influence the generation and separation of electron-hole pairs for photocatalytic reactions [5, 22].

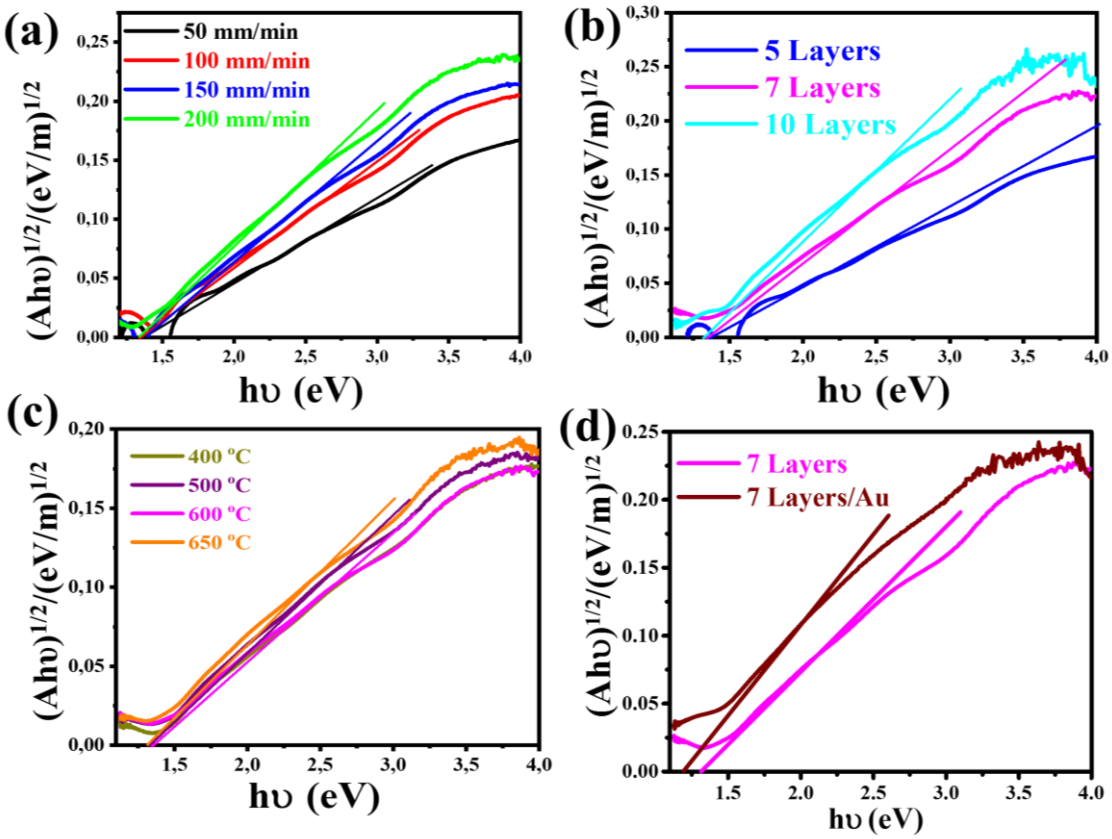

Fig. 8. Tauc approximation for the indirect bandgaps of CuO thin films **(a)** withdrawn from the precursor at different velocities, **(b)** consisting of different number of film layers, and **(c)** annealed at different temperatures: (d) compares the bandgaps of the pristine CuO and CuO/Au films.

3.5. Photoelectrochemical properties

LSV measurements were done to obtain the photocurrent response of the CuO films. Fig. 9 (a), (b), and (c) show the LSV results for measurements done on the CuO photocathodes under

dark and illumination conditions for samples prepared at several withdrawal rates, consisting of different film layers and annealed at various temperatures respectively. For samples prepared at varying withdrawal rates, the photocurrent increases with increasing withdrawal rate with values of 1.6 and 1.9 mA/cm^2 attained by the films prepared at 150 and 200mm/min respectively, at 0.35 V vs RHE. The enhanced crystallinity (Table 1) and photo-absorption (Fig. 7(a)) observed for the films prepared at higher withdrawal velocities contributed to the improved photocurrent density obtained for the films. The enhancement in the crystal sizes estimated for the films helped to promote the photocurrent response by decreasing the grain boundaries which often function as charge recombination sites on the surface of the films [43-45]. Furthermore, after the optimization of the film thickness and annealing temperature, the optimal photocurrent density of 2.9 mA/cm^2 at 0.35 V vs RHE was observed for the photocathodes prepared at 150 mm/min withdrawal velocity, made of 7 film layers and annealed at 600℃. This is higher than most of the photo-response reported for CuO photocathodes at 0.35 V vs RHE. The optimized film thickness of about 432.8 nm obtained for the films contributed to the maximal photocurrent density obtained. This was evident as a decline in photocurrent was observed for the photocathodes which were made to contain 10 film layers (Fig. 9(b)). Also, increasing annealing temperatures improve the grain size and crystallinity of the films, enhancing photocurrent response, until it reaches its maximum for films sintered at 600°C. Above this sintering temperature, the photocurrent density declined and generated 1.3 mA/cm^2 at 0.35 V vs RHE for films calcined at 650℃ [45-47]. In brief, the optimal photocurrent density observed for the CuO photocathodes is attributed to the combined effect of the optimization of the film thickness, optical absorption, and crystallinity of the films which promotes the photogeneration of charge carriers and transport during photocatalysis. An extremely low photocurrent was observed for the films sintered at 400°C. This has been ascribed to the poor crystallinity of the films which limit its charge mobility and the movement of electrons to the film's surface.

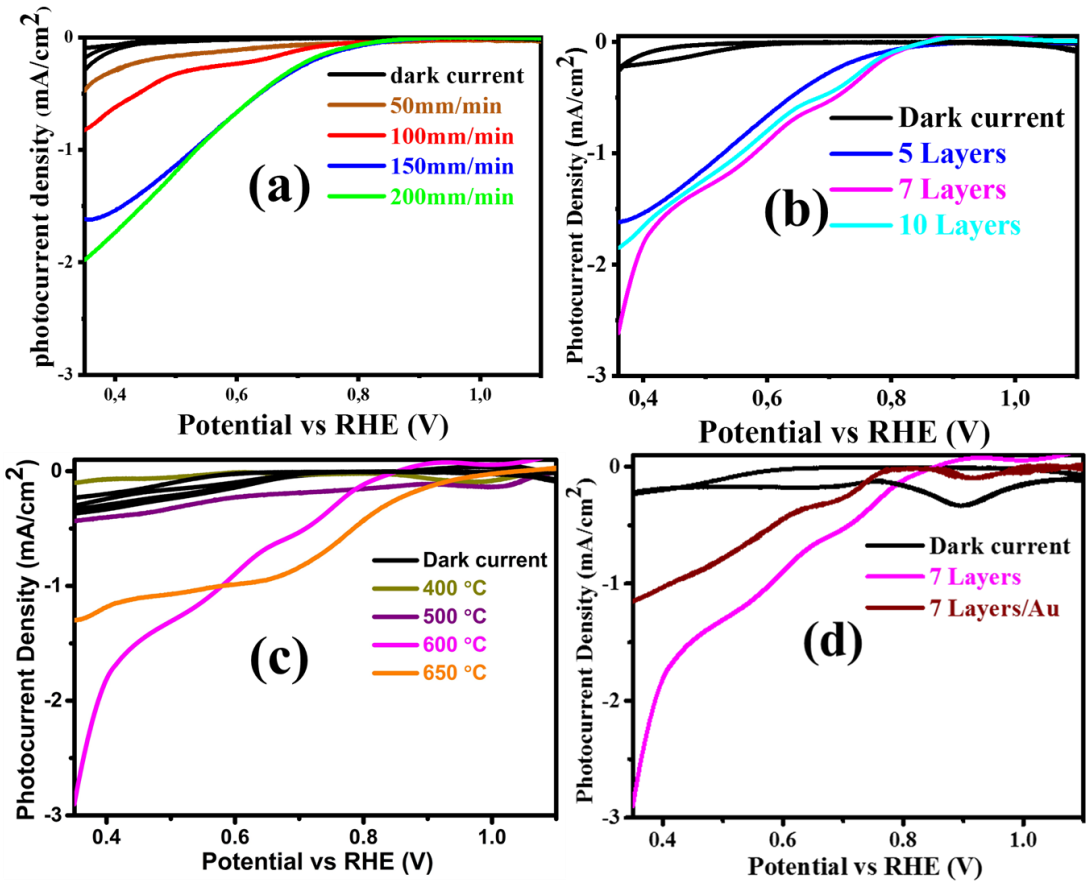

Fig. 9. Photocurrent density of CuO photocathodes **(a)** withdrawn from the precursor at different velocities, **(b)** consisting of varying number of film layers, and **(c)** annealed at various temperatures: (d) compares the photo response of the pristine CuO and CuO/Au films.

Table 2. Photocurrent response obtained for CuO films of different morphologies prepared using various methods after the optimization of certain processing parameters.

Material	**Structure**	**Fabrication Method / Processing parameter**	**Photocurrent response**	**Reference**
CuO	Nanoparticles	Sol-gel dip-coating / Film thickness.	2.9 mA/cm^2 at 0.35 V vs RHE, under 1 sun, and 1 M NaOH electrolyte.	**This project**
CuO	Nanocrystals	Electrodeposition / Deposition time.	0.23 mA/cm^2 at -0.3 V vs Ag/AgCl, under 8700 mW/m^2 irradiation (10 cm from sample), and 0.5 M Na_2SO_4 electrolyte.	[48]
CuO	Nanoleaves	aqueous solution / Precursor concentration.	1.5 mA/cm^2 at 0 V v/s RHE, under 100 mW/cm^2 irradiation, and 0.1 M Na2SO_4 electrolyte.	[49]

CuO	Nanosheets	aqueous solution / Concentration of the precursor.	1.1 mA/cm^2 at 0 V v/s RHE, under 100 mW/cm^2 irradiation, and 0.1 M Na_2SO_4 electrolyte.	[49]
CuO	pyramid structures	Electrodeposition / Deposition time.	-0.50 mA/cm^2 at 1.23 V vs Ag/AgCl, under 1 sun, and 0.5 M Na_2SO_4 electrolyte.	[44]
CuO	Nanoleaves	Hydrothermal / Irradiation time.	-1.50 mA/cm^2 at 0 V vs Ag/AgCl, under 1 sun, and 0.1 M Na_2SO_4 electrolyte.	[50]
CuO	Nanoparticles	RF-magnetron sputtering / Film thickness.	-3.1 mA/cm^2 at 0 V vs RHE, under 100 mW/cm^2 and AM 1.5 irradiation, and 0.1 M Na_2SO_4 electrolyte.	[51]
CuO	Nanoparticles	RF-magnetron sputtering / Film thickness	-3.88 mA/cm^2 at 0 V vs RHE, under 100 mW/cm^2 and AM 1.5 irradiation, and 0.1 M Na_2SO_4 electrolyte.	[51]
CuO	hollow spheres	doctor-blade / calcination temperature	-1.47 mA/cm^2 at -0.3 V vs Ag/AgCl, under 1 sun, and 0.5 M Na_2SO_4 electrolyte.	[52]
CuO	Nanowires	facile thermal treatment / calcination temperature	-1.4 mA/cm^2 at 0 V vs RHE, under 1 sun (100 mW/cm^2), and 1 M Na_2SO_4 electrolyte.	[4]

Photocurrent density of about 1.1 mA/cm^2 was observed for CuO/Au at 0.35 V vs RHE. This was 42.9 % less than the value obtained for the pristine films at the same potential. One of the limitations of using CuO in PEC applications is its high photo-corrosion rate which can also result in a current response during photocatalytic reactions [53]. The decrease in the photocurrent density of the CuO/Au photocathodes is attributed to the prevention of photo-corrosion by the Au protective layer. The Au layer significantly limits the current response of the pristine CuO films associated with corrosion under illumination. The photocurrent density obtain for the CuO/Au films in this work was larger than some reported values for the films in literature [54, 55]. The photocurrent of the CuO/Au photocathodes prepared in this study could be further improved by subjecting the deposited Au NPs to further heat treatment, at higher temperatures, and in an inert environment. This will potentially enhance the contact between the Au NPs and CuO which will promote charge transport at the interface between them and boast photocatalytic performance [56].

Fig. 10(a) present a schematic illustration of the photocatalytic reaction dynamics occurring on the surface of the CuO and photocathodes. The illumination of the CuO photocathodes with

solar radiation will lead to the production of electron-hole pairs in the bulk and surface of films. The holes eventually get drifted towards the FTO back contact while the electrons move towards the CuO surface where they engage in various reduction reactions. The H^+ ions in the electrolyte which are generated by the oxidation reaction occurring at the Pt counter electrode, reacts with the electrons at the surface of the CuO photocathodes to produce H_2. This is the desired reaction in PEC water splitting. However, due to the known poor stability of CuO in electrolyte, some of the electrons also go on to reduce the CuO films into Cu_2O and then to Cu if the reaction is sustained for a long period. The deposition of a protection layer such as Au on the surface of the CuO photocathodes will help in inhibiting the reduction of CuO by the surface electrons as illustrated in Fig. 10(b). The dominant reaction on the CuO/Au film surface is expected to be the reduction of H^+ to H_2, promoting the overall effectiveness of PEC water splitting by the photocathodes.

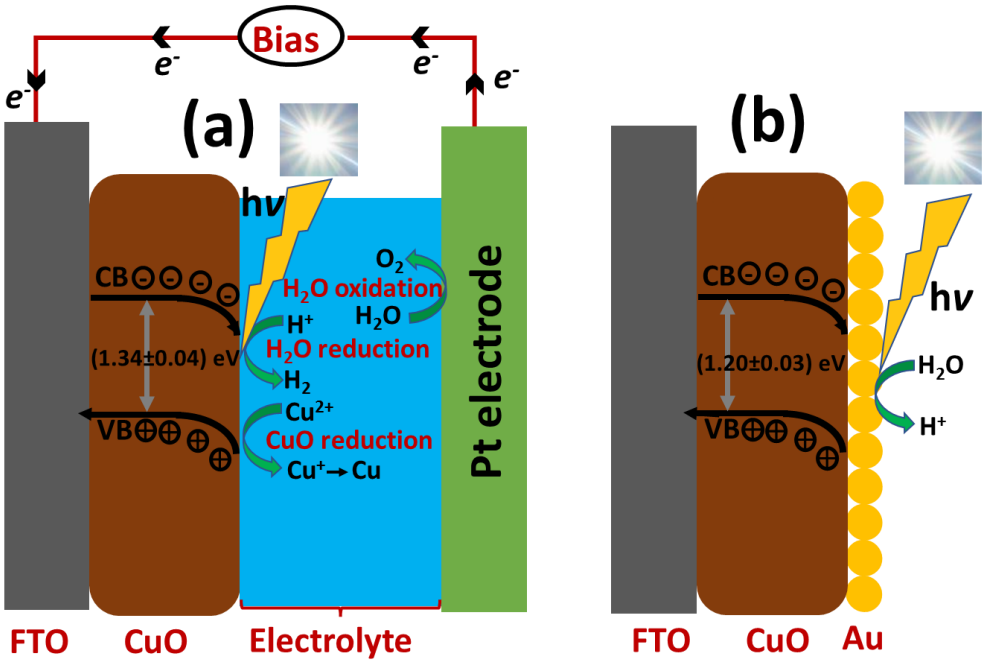

Fig. 10. Photocatalytic reactions occurring on the surface of (a) CuO and (b) CuO/Au photocathodes.

EIS was performed on the CuO and CuO/Au photocathodes to investigate the charge transfer processes occurring at the semiconductor/electrolyte interface. Fig. 11(a), (b), (c) shows the Nyquist plots of the experimental and fitted EIS data obtained for the samples prepared at different withdrawal rates, consisting of different film layers, and annealed at various

temperatures respectively. Fig. 10(d) shows a comparison between the Nyquist plot of CuO films that had 7-layers and the ones coated with a protective layer of Au. The circuit model engaged in fitting the measured EIS data of the films is given in the insets of Fig. 11(a)-(d). Rs represents the total series resistance caused by the FTO, electrolyte, and connecting wires and its value is equivalent to the intersection of the semi-circle with the real part of impendence [29, 57], whereas the Constant Phase Element (CPE) denotes the capacitance of the electric double-layer [58]. Rct refers to the resistance to the transfer of charges across the photocathode/electrolyte interface for hydrogen evolution reaction, and it is represented by the semi-circle diameters of the Nyquist plot. The smaller the semi-circle, the lower the charge transfer resistance [9, 57].

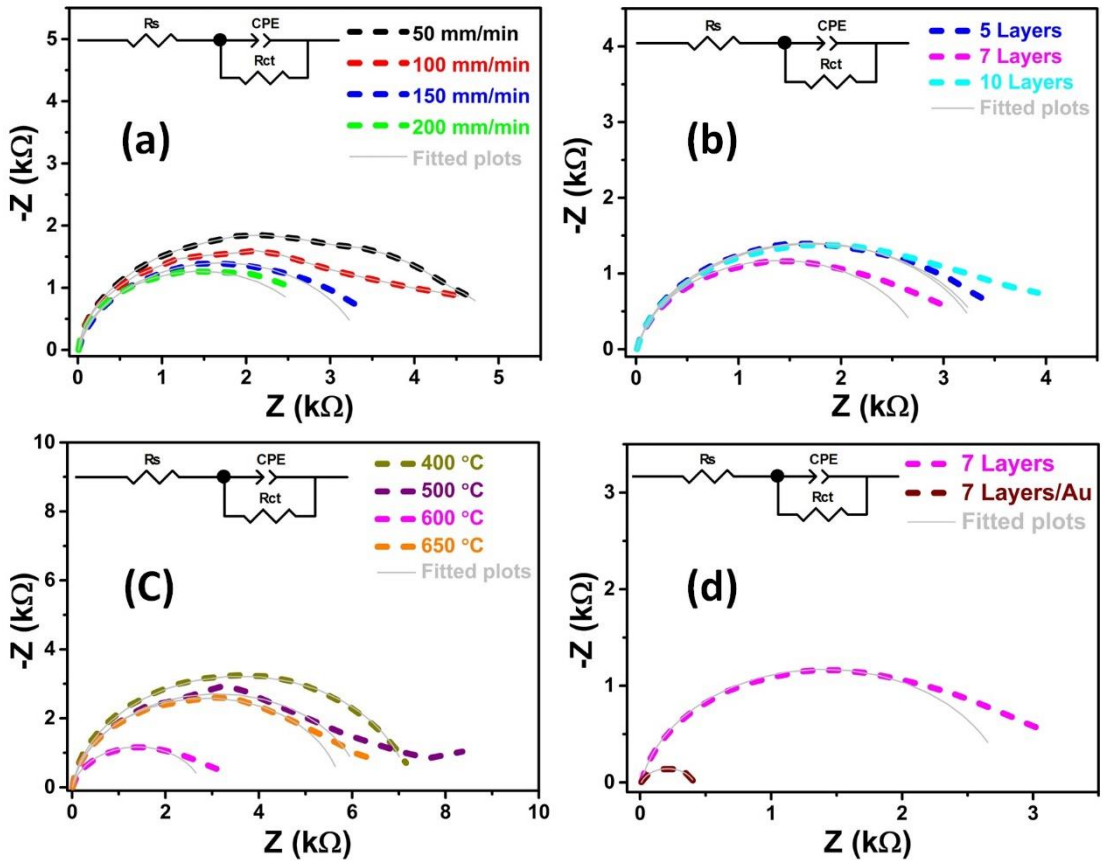

Fig. 11. EIS Nyquist plots of CuO photocathodes **(a)** withdrawn at different withdrawal velocities **(b)** consisting of varying number of film layers, and **(c)** annealed at various temperatures: (d) compares the Nyquist plot of pristine the CuO films with that of CuO/Au.

Upon fitting the modelled circuit to the raw EIS measurements, estimated values were obtained for the different elements and given in Table 3. For the pristine CuO films, the least Rct and

highest CPE values were attained by films deposited at 150 mm/min withdrawal velocity, made to contain 7 film layers and sintered at 600°C. Low Rct and high capacitance at the surface of the photocathodes can ease the movement of electrons at the solid/liquid interface during photocatalytic reactions [59]. This justifies the relatively large photocurrent density obtained for the CuO films made of 7 layers. Further modification of the pristine films consisting of 7 layers with Au nanoparticles resulted in an 88.4% drop in the charge transfer resistance of the films. The CPE values of the CuO/Au modified photocathodes was enhanced by a multiple factor of 3.3 when compared to that of the pristine films. However, despite having the lowest Rct values, the CuO/Au films yielded lower photocurrent densities as compared to the pristine CuO photocathodes (Fig. 9(d)). This was because a large part of the photocurrent observed for the pristine CuO films was due to photo-corrosion processes occurring on the films surface. The largest resistance to charge transfer was recorded by films treated at 400°C, which further clarifies the small photocurrent response exhibited by the films (Fig. 9(c)).

Table 3. The approximate values obtained for the different elements after fitting the EIS data obtained for the CuO and CuO/Au films to an equivalent circuit model.

Processing parameter	Sample	Rs (Ω)	Rct kΩ	CPE (µF)
Withdrawal rates	**50 mm/min**	8.39	4.42	35.4
	100 mm/min	9.16	3.74	40.4
	150 mm/min	9.25	3.38	70.1
	200 mm/min	9.02	2.89	36.1
Film layers	**5 Layers**	9.25	3.38	70.1
	7 Layers	9.71	2.79	89.3
	10 Layers	9.68	3.45	79.3
	7 Layers/Au	9.07	0.4	262.4
Annealing temperature	**400°C**	10.84	7.21	0.5
	500°C	10.00	6.20	38.6
	600°C	9.71	2.79	89.3
	650°C	10.33	5.76	0.5

The Mott-Schottky (MS) plots of the CuO and CuO/Au photocathodes are presented in Fig. 12. The approximate values of the flat-band potential (V_{FB}) and charge carrier concentration (N_A) estimated for the films were extracted from the plots, in line with the MS relation for photocathodes given in equation S1, and the results are presented in Table S2 of the supplementary data. The pristine CuO films produced a slightly higher flat-band potential value

of 1.049 V vs RHE which was about 18 mV more positive than the values obtained for the CuO/Au films. This contributed to the slightly earlier photocurrent onset potential observed for the pristine CuO films (Fig. 9(d)). The shift to a more negative flat band potential observed for the CuO/Au films may be attributed to the achieved equilibrium between the fermi levels of CuO and Au when the composite photocathodes were formed [60]. The charge carrier concentration of 5.64×10^{20} cm^{-3} was approximated for the CuO/Au films: an increment of over 6 times in comparison to the value obtained for the pristine films. The enhanced charge carrier concentration boosted charge mobility, transport, and reduce election-hole recombination in the bulk and surface of the CuO/Au photocathodes [15]. This further clarifies the reduced Rct value obtained for the CuO/Au photocathodes (Fig. 11(d)).

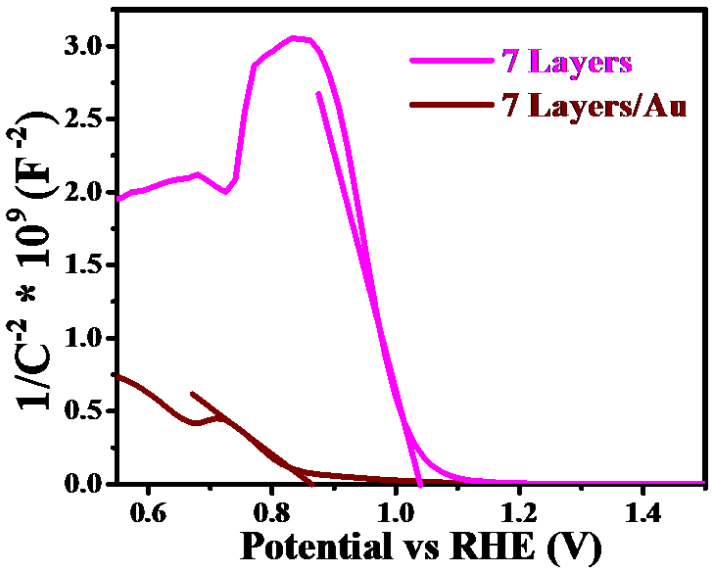

Fig. 12. The MS plots of CuO and CuO/Au photocathodes.

The stability of the pristine CuO thin films made of 7 film layers and the ones protected with Au NPs were studied using chronoamperometry measurements, at a constant potential of 0.6 V vs RHE, for a time scan of 500 s, and in the presence of 1 M NaOH electrolyte. Fig. 13 shows that the CuO films retained 58.7 and 28.4 % of their photocurrent density after 300 and 500 s respectively. This exhibition of poor stability in electrolyte by the CuO films was due to the high photo-corrosion caused by the self-reduction of CuO by photoexcited electrons. This is largely because the position of the thermodynamic reduction potential of CuO is below that of water [61-63]. This implies that the high photocurrent response observed for the CuO films (Fig. 9) will not be entirely due to the reduction of H^+ to hydrogen and the Faraday efficiencies

of the photocatalytic reactions are expected to be way below 100%. For instance, Cots *et al*., 2018 achieved Faraday efficiency of 45% for CuO films during photocatalysis because of their poor photostability [53]. Photo-corrosion is a limiting factor for the effective use of CuO as photocathodes for water reduction [61, 64]. This could be improved through doping with metal/non-metal ions [65], hetero-coupling [29], defect engineering [66], incorporation of passivation layers [67], deposition of protective layers of plasmonic metals [68], co-catalysts [69], and quantum dots [70] on the surface of the films, respectively. This was demonstrated in this work through the deposition of a protective layer of Au NPs on the CuO surface, which notably enhanced the photostability of the films in electrolyte. The CuO/Au films retained 87.9 and 85.1 % of their photocurrent after 300 and 500 s respectively. This represents a 3-fold improvement in the photo-stability of the films in electrolyte when compared to the 28.4% of the photocurrent retained by the pristine CuO photocathodes after the duration of 500 s. This also explains the drop in the photocurrent observed for the CuO/Au films when compared to that of the pristine films, since the Au modified photocathodes inhibited a significant portion of the current response associated with photo-corrosion. The CuO/Au photocathodes further exhibited good photostability after a potential-current scan of 1200 s, retaining 84.5% of its photocurrent response.

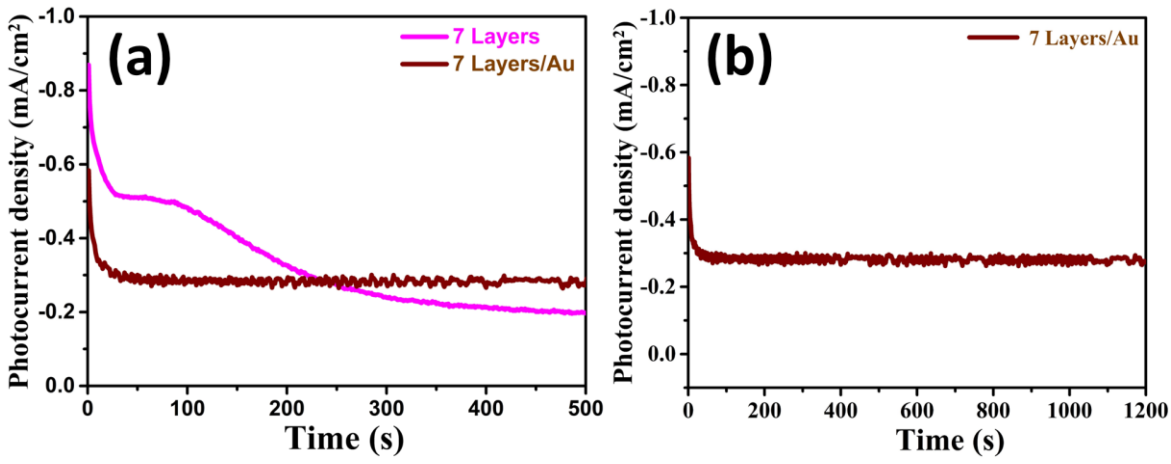

Fig. 13. Stability study conducted on CuO photocathode fabricated at 150 mm/min withdrawal velocity, consisting of 7 film layers, and calcined at 600℃.

4. Conclusion

In this study, the withdrawal velocity, film thickness, and calcination temperature for preparing dip-coated CuO photocathodes were optimized for PEC water-splitting. CuO photocathodes were prepared at different withdrawal velocities between 50-200 mm/min, made to consist of 239.7–693.6 ± 40 nm film thicknesses, and annealed at 400-650°C for 1 hr. In addition, Au nanoparticles were also deposited on the pristine CuO films that was 432.8 ± 40 nm thick and treated at 600°C, to protect the films against photo-corrosion during PEC reactions. The XRD pattern and Raman spectra confirmed the preparation of crystalline CuO and CuO/Au films. The surface morphology of the thin films disclosed compact spherical nanoparticles while their cross-sectional images exhibited an increase in film thickness with increasing withdrawal velocity and number of film layers. EDS studies affirmed the presence of O and Cu in the CuO films and also detected the Au NPs deposited on the pristine films. The CuO and CuO/Au films exhibited good optical absorption within the visible spectrum with some slight absorption in the near-infrared region due to their estimated low bandgap of 1.34 $\pm$ 0.04 eV and 1.20 ± 0.03 eV respectively. LSV measurements yielded the highest photocurrent density of was 2.9 mA/cm^2 at 0.35 V vs RHE, attained by films prepared at 150 mm/min withdrawal velocity, with the thickness of 432.8 nm, and sintered at 600°C. The improved photocurrent density attained by the films has been linked to the optimization of the film's thickness, optical absorbance, crystallization, and the low resistance to the transfer of charge carriers at the photocathode/electrolyte interface. The deposition of Au NPs on the pristine CuO films resulted in a 62 % drop in their photocurrent density. This has been attributed to the inhibition of high photo-corrosion occurring on the surface of the pristine films. A potential-time scan at 0.6V vs RHE for 500 s yielded a 3-fold improvement in the photo-stability of the Au coated films over the pristine CuO photocathodes. This study emphasized the significance of optimizing multiple processing parameters in the development of CuO films and the deposition of protective layers on the films for PEC applications.

Acknowledgments

The authors acknowledge support from the University of Pretoria (UP) and funding from the National Research Foundation, the UP postdoctoral fellowship programme: grant DRI - cost centre: A0X816, and the South African Research Chairs Initiative (SARCHI), UID; 115463.

References

[1] J. Bongaarts and B. C. O'Neill, "Global warming policy: Is population left out in the cold?," *Science,* vol. 361, no. 6403, pp. 650-652, 2018.

[2] T. Veziro and F. Barbir, "Hydrogen: the wonder fuel," *International Journal of Hydrogen Energy,* vol. 17, no. 6, pp. 391-404, 1992.

[3] I. Dincer and C. Acar, "Review and evaluation of hydrogen production methods for better sustainability," *International journal of hydrogen energy,* vol. 40, no. 34, pp. 11094-11111, 2015.

[4] J. Li *et al.*, "Copper oxide nanowires for efficient photoelectrochemical water splitting," *Appl. Catal., B,* vol. 240, pp. 1-8, 2019.

[5] Z. Wang and L. Wang, "Photoelectrode for water splitting: Materials, fabrication and characterization," *Science China Materials,* vol. 61, no. 6, pp. 806-821, 2018.

[6] T. Hisatomi, J. Kubota, and K. Domen, "Recent advances in semiconductors for photocatalytic and photoelectrochemical water splitting," *Chemical Society Reviews,* vol. 43, no. 22, pp. 7520-7535, 2014.

[7] S. Wang, P. Chen, Y. Bai, J. H. Yun, G. Liu, and L. Wang, "New BiVO4 Dual Photoanodes with Enriched Oxygen Vacancies for Efficient Solar-Driven Water Splitting," *Advanced Materials,* vol. 30, no. 20, p. 1800486, 2018.

[8] W. Yang and J. Moon, "Recent advances in earth-abundant photocathodes for photoelectrochemical water splitting," *ChemSusChem,* vol. 12, no. 9, pp. 1889-1899, 2019.

[9] J. Toupin, H. Strubb, S. Kressman, V. Artero, N. Krins, and C. Laberty-Robert, "CuO photoelectrodes synthesized by the sol–gel method for water splitting," *J. Sol-Gel Sci. Technol.,* vol. 89, no. 1, pp. 255-263, 2019.

[10] G. Papadimitropoulos, N. Vourdas, V. E. Vamvakas, and D. Davazoglou, "Optical and structural properties of copper oxide thin films grown by oxidation of metal layers," *Thin Solid Films,* vol. 515, no. 4, pp. 2428-2432, 2006.

[11] A. Bhaduri and Kajal, "Facile synthesis and characterization of cupric oxide (CuO) nanoparticles: Inexpensive and abundant candidate for light harvesting," in *AIP Conference Proceedings*, 2019, vol. 2093, no. 1: AIP Publishing LLC, p. 020047.

[12] H. L. Santos, P. G. Corradini, M. A. Andrade, and L. H. Mascaro, "CuO/NiO x thin film–based photocathodes for photoelectrochemical water splitting," *Journal of Solid State Electrochemistry*, pp. 1-10, 2020.

[13] Z. Guo and Z. Liu, "Synthesis and control strategies of nanomaterials for photoelectrochemical water splitting," *Dalton Transactions,* 2021.

[14] P. Kumar, P. Sharma, R. Shrivastav, S. Dass, and V. R. Satsangi, "Electrodeposited zirconium-doped α-Fe2O3 thin film for photoelectrochemical water splitting," *international journal of hydrogen energy,* vol. 36, no. 4, pp. 2777-2784, 2011.

[15] N. A. Arzaee *et al.*, "Aerosol-assisted chemical vapour deposition of α-Fe2O3 nanoflowers for photoelectrochemical water splitting," *Ceram. Int.*, vol. 45, no. 14, pp. 16797-16802, 2019.

[16] H. B. Saâd, M. Ajili, S. Dabbabi, and N. T. Kamoun, "Investigation on thickness and annealing effects on physical properties and electrical circuit model of CuO sprayed thin films," *Superlattices and Microstructures*, vol. 142, p. 106508, 2020.

[17] R. Bashiri, N. M. Mohamed, and C. F. Kait, "Advancement of sol-gel–prepared TiO2 photocatalyst," *Recent Applications in Sol-Gel Synthesis. Rijeka: InTech*, pp. 151-167, 2017.

[18] Z. N. Kayani, A. Aslam, R. Ishaque, S. N. Zahra, H. Hanif, and H. Khan, "The effect of the withdrawal speed on properties of nickel oxide thin films," *Zeitschrift für Kristallographie-Crystalline Materials*, vol. 234, no. 10, pp. 647-655, 2019.

[19] R. Sathyamoorthy, C. Sharmila, K. Natarajan, and S. Velumani, "Influence of annealing on structural and optical properties of Zn3P2 thin films," *Materials characterization*, vol. 58, no. 8-9, pp. 745-749, 2007.

[20] S. Aydemir, "Effects of withdrawal speed on the microstructural and optical properties of sol–gel grown ZnO: Al thin films," *Vacuum*, vol. 120, pp. 51-58, 2015.

[21] J. Joy, J. Mathew, and S. C. George, "Nanomaterials for photoelectrochemical water splitting–review," *Int. J. Hydrogen Energy*, vol. 43, no. 10, pp. 4804-4817, 2018.

[22] A. Kudo and Y. Miseki, "Heterogeneous photocatalyst materials for water splitting," *Chem. Soc. Rev.*, vol. 38, no. 1, pp. 253-278, 2009.

[23] F. A. Akgul, G. Akgul, N. Yildirim, H. E. Unalan, and R. Turan, "Influence of thermal annealing on microstructural, morphological, optical properties and surface electronic structure of copper oxide thin films," *Materials Chemistry and Physics*, vol. 147, no. 3, pp. 987-995, 2014.

[24] A. Musaa, S. Farhad, M. Gafura, and A. Jamilb, "Effects of withdrawal speeds on the structural, morphological, electrical, and optical properties of CuO thin films synthesized by dip-coating for CO2 gas sensing."

[25] S. Shariffudin, S. Khalid, N. Sahat, M. Sarah, and H. Hashim, "Preparation and characterization of nanostructured CuO thin films using sol-gel dip coating," in *IOP Conference Series: Materials Science and Engineering*, 2015, vol. 99, no. 1: IOP Publishing, p. 012007.

[26] N. Raship, M. Sahdan, F. Adriyanto, M. Nurfazliana, and A. Bakri, "Effect of annealing temperature on the properties of copper oxide films prepared by dip coating technique," in *AIP Conference Proceedings*, 2017, vol. 1788, no. 1: AIP Publishing, p. 030121.

[27] P. I. Kyesmen, N. Nombona, and M. Diale, "A Promising Three-Step Heat Treatment Process for Preparing CuO Films for Photocatalytic Hydrogen Evolution from Water," *ACS Omega*, 2021.

[28] R. Van de Krol and M. Grätzel, *Photoelectrochemical hydrogen production*. Springer, 2012.

[29] P. I. Kyesmen, N. Nombona, and M. Diale, "Heterojunction of nanostructured α-Fe2O3/CuO for enhancement of photoelectrochemical water splitting," *J. Alloys Compd.,* vol. 863, p. 158724, 2021.

[30] C. Brinker, G. Frye, A. Hurd, and C. Ashley, "Fundamentals of sol-gel dip coating," *Thin solid films,* vol. 201, no. 1, pp. 97-108, 1991.

[31] Y. Akaltun, "Effect of thickness on the structural and optical properties of CuO thin films grown by successive ionic layer adsorption and reaction," *Thin Solid Films,* vol. 594, pp. 30-34, 2015.

[32] P. I. Kyesmen, N. Nombona, and M. Diale, "Influence of coating techniques on the optical and structural properties of hematite thin films," *Surfaces and Interfaces,* vol. 17, p. 100384, 2019.

[33] P. Peerakiatkhajohn, J.-H. Yun, S. Wang, and L. Wang, "Review of recent progress in unassisted photoelectrochemical water splitting: from material modification to configuration design," *Journal of Photonics for Energy,* vol. 7, no. 1, p. 012006, 2016.

[34] P. I. Kyesmen, N. Nombona, and M. Diale, "Modified annealing approach for preparing multi-layered hematite thin films for photoelectrochemical water splitting," *Mater. Res. Bull.,* vol. 131, p. 110964, 2020.

[35] W. Wang, Z. Liu, Y. Liu, C. Xu, C. Zheng, and G. Wang, "A simple wet-chemical synthesis and characterization of CuO nanorods," *Applied Physics A,* vol. 76, no. 3, pp. 417-420, 2003.

[36] J. Sultana, S. Paul, A. Karmakar, G. K. Dalapati, and S. Chattopadhyay, "Optimizing the thermal annealing temperature: technological route for tuning the photo-detecting property of p-CuO thin films grown by chemical bath deposition method," *Journal of Materials Science: Materials in Electronics,* vol. 29, no. 15, pp. 12878-12887, 2018.

[37] C. J. Brinker and G. W. Scherer, *Sol-gel science: the physics and chemistry of sol-gel processing*. Academic press, 2013.

[38] O. Zandi, J. A. Beardslee, and T. Hamann, "Substrate dependent water splitting with ultrathin α-Fe2O3 electrodes," *The Journal of Physical Chemistry C,* vol. 118, no. 30, pp. 16494-16503, 2014.

[39] S. Kumari *et al.,* "Combinatorial synthesis and high-throughput characterization of Fe–V–O thin-film materials libraries for solar water splitting," *ACS combinatorial science,* vol. 20, no. 9, pp. 544-553, 2018.

[40] L. Landau and B. Levich, "" Dragging of a Liquid by a Moving Plate, " ActaPhysicochimica," ed: URSS, 1942.

[41] J. Puetz and M. Aegerter, "Dip coating technique," in *Sol-Gel Technologies for Glass Producers and Users*: Springer, 2004, pp. 37-48.

[42] J. Tauc, "The optical properties of solids," *The Optical Properties of Solids,* 1966.

[43] S. Masudy-Panah *et al.*, "Nanocrystal engineering of sputter-grown CuO photocathode for visible-light-driven electrochemical water splitting," *ACS Appl. Mater. Interfaces,* vol. 8, no. 2, pp. 1206-1213, 2016.

[44] A. Mahmood, F. Tezcan, and G. Kardaş, "Photoelectrochemical characteristics of CuO films with different electrodeposition time," *Int. J. Hydrogen Energy,* vol. 42, no. 36, pp. 23268-23275, 2017.

[45] S. Masudy-Panah, R. S. Moakhar, C. S. Chua, A. Kushwaha, T. I. Wong, and G. K. Dalapati, "Rapid thermal annealing assisted stability and efficiency enhancement in a sputter deposited CuO photocathode," *RSC Adv.,* vol. 6, no. 35, pp. 29383-29390, 2016.

[46] M. Lamers, S. Fiechter, D. Friedrich, F. F. Abdi, and R. van de Krol, "Formation and suppression of defects during heat treatment of BiVO 4 photoanodes for solar water splitting," *Journal of Materials Chemistry A,* vol. 6, no. 38, pp. 18694-18700, 2018.

[47] F. Du, Q.-Y. Chen, and Y.-H. Wang, "Effect of annealing process on the heterostructure CuO/Cu2O as a highly efficient photocathode for photoelectrochemical water reduction," *Journal of Physics and Chemistry of Solids,* vol. 104, pp. 139-144, 2017.

[48] C. S. Yaw, A. K. Soh, and M. N. Chong, "Effect of deposition time on the photoelectrochemical properties of cupric oxide thin films synthesized via electrodeposition method," in *MATEC Web of Conferences,* 2016, vol. 60: EDP Sciences, p. 01001.

[49] A. Kushwaha, R. S. Moakhar, G. K. Goh, and G. K. Dalapati, "Morphologically tailored CuO photocathode using aqueous solution technique for enhanced visible light driven water splitting," *Journal of Photochemistry and Photobiology A: Chemistry,* vol. 337, pp. 54-61, 2017.

[50] R. S. Moakhar, F. Soleimani, A. Goudarzi, and S. K. Sadrnezhaad, "A Novel Method to Fabricate Hierarchical Copper Oxide Photoelectrode and Its Application for Photoelectrochemical Water Splitting," *ECS Trans.,* vol. 97, no. 7, p. 845, 2020.

[51] S. Masudy-Panah, R. Siavash Moakhar, C. S. Chua, A. Kushwaha, and G. K. Dalapati, "Stable and efficient CuO based photocathode through oxygen-rich composition and Au–Pd nanostructure incorporation for solar-hydrogen production," *ACS Appl. Mater. Interfaces,* vol. 9, no. 33, pp. 27596-27606, 2017.

[52] Y.-H. Choi, D.-H. Kim, H. S. Han, S. Shin, S.-H. Hong, and K. S. Hong, "Direct printing synthesis of self-organized copper oxide hollow spheres on a substrate using copper (II) complex ink: Gas sensing and photoelectrochemical properties," *Langmuir,* vol. 30, no. 3, pp. 700-709, 2014.

[53] A. Cots, P. Bonete, and R. Gómez, "Improving the stability and efficiency of CuO photocathodes for solar hydrogen production through modification with iron," *ACS Appl. Mater. Interfaces,* vol. 10, no. 31, pp. 26348-26356, 2018.

[54] X. Zhang, Y. Yang, W. Que, and Y. Du, "Synthesis of high quality CuO nanoflakes and CuO–Au nanohybrids for superior visible light photocatalytic behavior," *RSC Adv.*, vol. 6, no. 85, pp. 81607-81613, 2016.

[55] K.-A. Tsai and Y.-J. Hsu, "Preparation and Photoelectrochemical Property of Au-CuO Heterodimer Nanostructures," in *ECS Meeting Abstracts*, 2011, no. 18: IOP Publishing, p. 1549.

[56] L. Wang *et al.*, "Simultaneously efficient light absorption and charge transport of CdS/TiO2 nanotube array toward improved photoelectrochemical performance," *Int. J. Hydrogen Energy*, vol. 44, no. 59, pp. 30899-30909, 2019.

[57] Y. Chen, A. Li, Q. Li, X. Hou, L.-N. Wang, and Z.-H. Huang, "Facile fabrication of three-dimensional interconnected nanoporous N-TiO2 for efficient photoelectrochemical water splitting," *Journal of materials science & technology*, vol. 34, no. 6, pp. 955-960, 2018.

[58] P. Córdoba-Torres, T. J. Mesquita, and R. P. Nogueira, "Relationship between the origin of constant-phase element behavior in electrochemical impedance spectroscopy and electrode surface structure," *The Journal of Physical Chemistry C*, vol. 119, no. 8, pp. 4136-4147, 2015.

[59] P. Jubu, F. Yam, and P. I. Kyesmen, "Structural, optical and electrochemical transient photoresponse properties of ZnO/Ga2O3 nanocomposites prepared by two-step CVD method," *Int. J. Hydrogen Energy*, 2021.

[60] G. Hu, C.-X. Hu, Z.-Y. Zhu, L. Zhang, Q. Wang, and H.-L. Zhang, "Construction of Au/CuO/Co3O4 tricomponent heterojunction nanotubes for enhanced photocatalytic oxygen evolution under visible light irradiation," *ACS Sustainable Chemistry & Engineering*, vol. 6, no. 7, pp. 8801-8808, 2018.

[61] H. Xing, E. Lei, Z. Guo, D. Zhao, X. Li, and Z. Liu, "Exposing the photocorrosion mechanism and control strategies of a CuO photocathode," *Inorganic Chemistry Frontiers*, vol. 6, no. 9, pp. 2488-2499, 2019.

[62] M. Basu, "Porous cupric oxide: efficient photocathode for photoelectrochemical water splitting," *ChemPhotoChem*, vol. 3, no. 12, pp. 1254-1262, 2019.

[63] H. Gerischer, "On the stability of semiconductor electrodes against photodecomposition," *Journal of Electroanalytical Chemistry and Interfacial Electrochemistry*, vol. 82, no. 1-2, pp. 133-143, 1977.

[64] H. Tang *et al.*, "Enhancing the stability of CuO thin-film photoelectrodes by Ti alloying," *Journal of electronic materials*, vol. 41, no. 11, pp. 3062-3067, 2012.

[65] A. Ranjitha, N. Muthukumarasamy, M. Thambidurai, D. Velauthapillai, R. Balasundaraprabhu, and S. Agilan, "Fabrication of Ni-doped TiO2 thin film photoelectrode for solar cells," *Solar energy*, vol. 106, pp. 159-165, 2014.

[66] Z. Wang *et al.*, "Identifying copper vacancies and their role in the CuO based photocathode for water splitting," *Angewandte Chemie*, vol. 131, no. 49, pp. 17768-17773, 2019.

[67] R. Liu, Z. Zheng, J. Spurgeon, and X. Yang, "Enhanced photoelectrochemical water-splitting performance of semiconductors by surface passivation layers," *Energy & Environmental Science,* vol. 7, no. 8, pp. 2504-2517, 2014.

[68] G. S. Pawar, A. Elikkottil, B. Pesala, A. A. Tahir, and T. K. Mallick, "Plasmonic nickel nanoparticles decorated on to LaFeO3 photocathode for enhanced solar hydrogen generation," *International Journal of Hydrogen Energy,* vol. 44, no. 2, pp. 578-586, 2019.

[69] S. Pokrant, S. Dilger, S. Landsmann, and M. Trottmann, "Size effects of cocatalysts in photoelectrochemical and photocatalytic water splitting," *Materials Today Energy,* vol. 5, pp. 158-163, 2017.

[70] S. R. AR, B. M. Momin, H. M. Wilson, U. S. Annapure, and N. Jha, "Optimal fabrication of 0D/1D Cu2O quantum dots sensitized CdS nanorods heterojunction: Efficient photoredox catalyst for H2 generation under visible light irradiation," *Journal of Alloys and Compounds,* vol. 835, p. 155262, 2020.